ELSEVIER

Journal of Alloys and Compounds 449 (2008) 119–124

Journal of ALLOYS AND COMPOUNDS

www.elsevier.com/locate/jallcom

Aging effect on a $Ti_{47.25}Ni_{48.75}V_4$ shape memory alloy

H.C. Lin [a,*], C.H. Yang [b], M.C. Lin [c], C.S. Lin [a], K.M. Lin [b], L.S. Chang [c]

[a] *Department of Materials Science and Engineering, National Taiwan University, Taipei, Taiwan*
[b] *Department of Materials Science and Engineering, Feng Chia University, Taichung, Taiwan*
[c] *Department of Materials Engineering, National ChungHsing University, Taichung, Taiwan*

Received 4 November 2005; received in revised form 29 December 2005; accepted 16 January 2006
Available online 12 January 2007

Abstract

Aging effect on a $Ti_{47.25}Ni_{48.75}V_4$ shape memory alloy is investigated. Experimental results reveal that the 400 °C aged $Ti_{47.25}Ni_{48.75}V_4$ alloy exhibits a B2 → R → B19′ two-stage martensitic transformation on cooling, but exhibits a B19′ → B2 one-stage transformation on heating. Two kinds of second phases, $(Ti,V)_2Ni$ and $V_9(Ti,Ni)$, are observed in the solution-treated $Ti_{47.25}Ni_{48.75}V_4$ alloy. $(Ti,V)_2Ni$ exhibits an FCC order structure with a lattice parameter of 11.1 Å while $V_9(Ti,Ni)$ exhibits a BCC structure with a lattice parameter of 3.01 Å. There appear lots of fine spherical $V_9(Ti,Ni)$ and coherent Ti_3Ni_4 precipitates after 400 °C aging for the $Ti_{47.25}Ni_{48.75}V_4$ alloy. These precipitates will strengthen the alloy's matrix and improve the shape recovery ability.

Keywords: TiNiV shape memory alloy; Martensitic transformation; Aging treatment

1. Introduction

Among many shape memory alloys, TiNi alloys are the most popular because they have superior properties in shape memory effect (SME) [1] and pseudoelasticity (PE) [2,3] applications. The transformation behaviors and mechanical properties in TiNi binary alloys can be affected by various thermo-mechanical treatments, such as thermal cycling [4,5], aging in Ni-rich alloys [6,7], and annealing after cold working [8,9]. Furthermore, the addition of a third element has a substantial effect on phase transformation behavior in TiNi alloys. The Ms temperature decreases monotonously following substitution of Ni with Cr, Mn, Fe, and Co elements [10,11], but increase remarkably following substitution of Ni with Au, Pd, and Pt in amounts not less than 15–20 at.% [12,13]. On the other hand, the addition of Nb into TiNi alloy can widen the transformation hysteresis (As to Ms) to above 130 °C, and hence extend the application of coupling and sealing [14]. In our previous article [15], the $Ti_{49.25-X/2}Ni_{50.75-X/2}V_X$ ($X = 0$–4 at.%) ternary shape memory alloys, obtained by equal substitution of V for both Ti and Ni, were investigated, which focused on their basic properties, including the transformation behavior, shape memory effect, pseudoelasticity and wear resistance. It was found that the slight addition of V element into TiNi alloys could significantly affect their transformation temperatures, SME and PE properties. In the present study, we continue to investigate the aging effect on a $Ti_{47.25}Ni_{48.75}V_4$ alloy, including the variations of transformation behavior, microstructure and shape memory effect.

2. Experimental

The conventional tungsten arc-melting technique was employed to prepare the $Ti_{47.25}Ni_{48.75}V_4$ alloy. Titanium (99.7 wt%), nickel (99.98 wt%) and vanadium (99.7 wt%), totaling about 100 g, were melted and remelted at least eight times in an argon atmosphere. The as-melted button was homogenized at 1050 °C for 24 h, quenched in water, and then hot-rolled at 800 °C to a plate with 3-mm thickness. Specimens for the differential scanning calorimetry (DSC) measurement, shape recovery testing, TEM observation and hardness measurement were carefully cut from this plate with a low speed-diamond saw. These specimens were sealed and evacuated in quartz tubes, annealed at 800 °C for 2 h, and quenched in water. Then they were aged in a salt-bath at 400 °C for 1–10 h and again quenched in water.

The DSC measurement was conducted with a DuPont 2000 thermal analyzer equipped with a quantitative scanning system 910 DSC cell. The cooling/heating rate was precisely controlled at 5 °C/min. The shape recovery ability was examined by a bending test, as illustrated in a previous paper [16]. TEM specimens were prepared by jet electro-polishing at room temperature with an electrolyte consisting of 20% H_2SO_4 and 80% CH_3OH by volume. TEM observation was carried out by using a JEOL-400 FX microscope equipped

* Corresponding author. Tel.: +886 2 3366 4532; fax: +886 2 2363 4562.
E-mail address: hclinntu@ntu.edu.tw (H.C. Lin).

0925-8388/$ – see front matter © 2006 Elsevier B.V. All rights reserved.
doi:10.1016/j.jallcom.2006.01.136

with an EDS facility. Specimens for hardness measurements were mechanically polished and measured in a microvickers hardness tester with a 500-g load. For each specimen, the average hardness value was obtained from at least five test readings.

3. Results and discussion

3.1. Transformation behavior

The martensitic transformation behavior, involving transformation sequence and temperatures, can be measured by using the DSC method. Fig. 1(a) represents a typical DSC curve of the solution-treated $Ti_{47.25}Ni_{48.75}V_4$ specimen in which the exothermic and endothermic peaks are associated with the martensitic transformation, B2 ↔ B19′. Fig. 1(b–d) shows the DSC curves of the $Ti_{47.25}Ni_{48.75}V_4$ specimens aged at 400 °C for 1, 5 and 10 h, respectively. In Fig. 1(b–d), the DSC curves exhibit a B2 → R → B19′ two-stage martensitic transformation on cooling, but a B19′ → B2 one-stage transformation on heating. This phenomenon is more obvious for the 400 °C × 5 h and 400 °C × 10 h aged specimens. It indicates that the R-phase transformation occurs before the martensitic transformation on cooling. This feature is similar to the aging behavior of Ni-rich TiNi binary alloys [6], although the DSC peaks of the R-phase and martensitic transformations in the 400 °C aged $Ti_{47.25}Ni_{48.75}V_4$ specimens are not so separated. It is well known [6,17–20] that the R-phase transformation is related to the formation of Ti_3Ni_4 precipitates during aging. The coherent stress around the boundaries between Ti_3Ni_4 precipitates and B2 matrix will hinder the martensitic transformation and hence introduce the R-phase transformation on cooling. However, there only appears a B19′ → B2 reverse martensitic transformation on heating. It indicates that the residual stress around the boundaries of Ti_3Ni_4 precipitates and B19′ martensite is not sufficient to introduce the B19′ → R-phase transformation on heating for the 400 °C aged $Ti_{47.25}Ni_{48.75}V_4$ specimens. As carefully examining the DSC curves in Fig. 1(a–d), the transformation temperatures for the R-phase and martensitic transformations are found to slightly increase with increasing aging time. This feature is believed to be related to the variation of Ni/Ti ratio in the matrix after 400 °C aging. Due to the formation of Ti_3Ni_4 precipitates, the Ni/Ti ratio in the matrix decreases and hence the transformation temperatures increase.

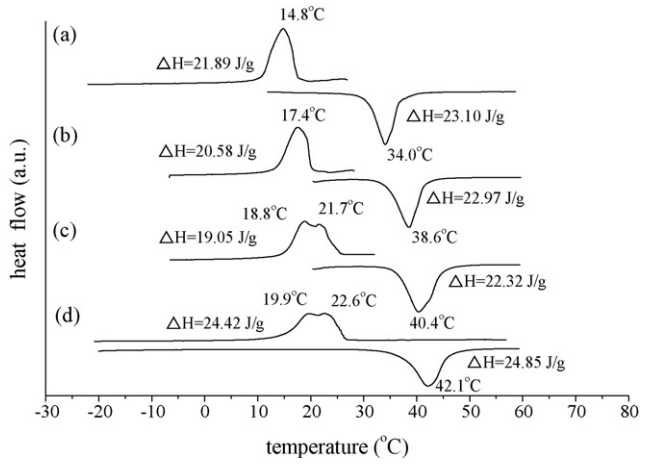

Fig. 1. DSC curves for the 400 °C aged $Ti_{47.25}Ni_{48.75}V_4$ alloy. (a) S.T., (b) 400 °C × 1 h, (c) 400 °C × 5 h, and (d) 400 °C × 10 h.

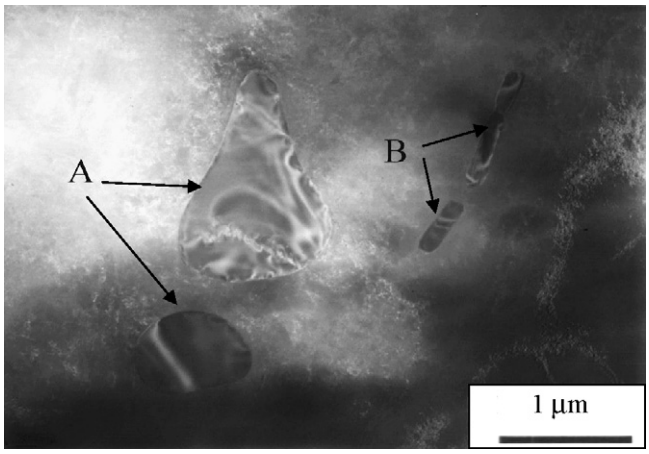

Fig. 2. TEM observation showing the appearance of second-phase A and B in the solution-treated $Ti_{47.25}Ni_{48.75}V_4$ alloy.

3.2. TEM observation and analysis

Fig. 2 shows the TEM observation of solution-treated $Ti_{47.25}Ni_{48.75}V_4$ alloy. Two kinds of second phase within the austenitic matrix are observed, indicated as A and B in Fig. 2. A is bigger and near-spherical, and B has a shape of long-strip. Figs. 3 and 4 show the bright-field image, selected area diffraction pattern (SADP) and TEM-EDS composition analysis of the second-phases A and B, respectively. According to the analysis of Fig. 3(a–e), the A phase has an FCC order structure with lattice parameter of 11.1 Å, and its compositions are analyzed to be 61.14 at.% Ti, 34.79 at.% Ni, 4.07 at.% V, namely, the A phase is the $(Ti,V)_2Ni$ compound. Whilst, the analysis of Fig. 4(a–e) shows that the B phase has a BCC structure with lattice parameter of 3.01 Å, and its compositions are analyzed to be 4.89 at.% Ti, 4.07 at.% Ni, 90.51 at.% V, namely, the B phase is identified to be the $V_9(Ti,Ni)$. The Ti_2Ni compound is often observed in the Ti–Ni shape memory alloys [21]. However, to the best of authors' knowledge, there is no report about the $V_9(Ti,Ni)$ phase, even not been observed in the Ti–Ni–V ternary phase diagram. The compositions of the matrix detected are about 46.40 at.% Ti, 50.69 at.% Ni, 2.91 at.% V. The content of V atoms in the matrix is less than the nominal composition of 4 at.%. This phenomenon is reasonable because lots of V atoms are consumed in forming the $V_9(Ti,Ni)$ phase. In other words, the solubility limit of V atoms within the matrix of this alloy solution-treated at 800 °C is about 2.91 at.%. The extra amount of V atoms will form the $V_9(Ti,Ni)$ phase. In Figs. 3 and 4, the bright-field images show that the A phase appears within the grains, and the B phase is mainly observed along the grain boundaries.

It is well known that the Ni-rich Ti–Ni binary alloys will produce the Ti_3Ni_4 precipitates after aging treatment [6,17–20]. These Ti_3Ni_4 precipitates will have significant influence on

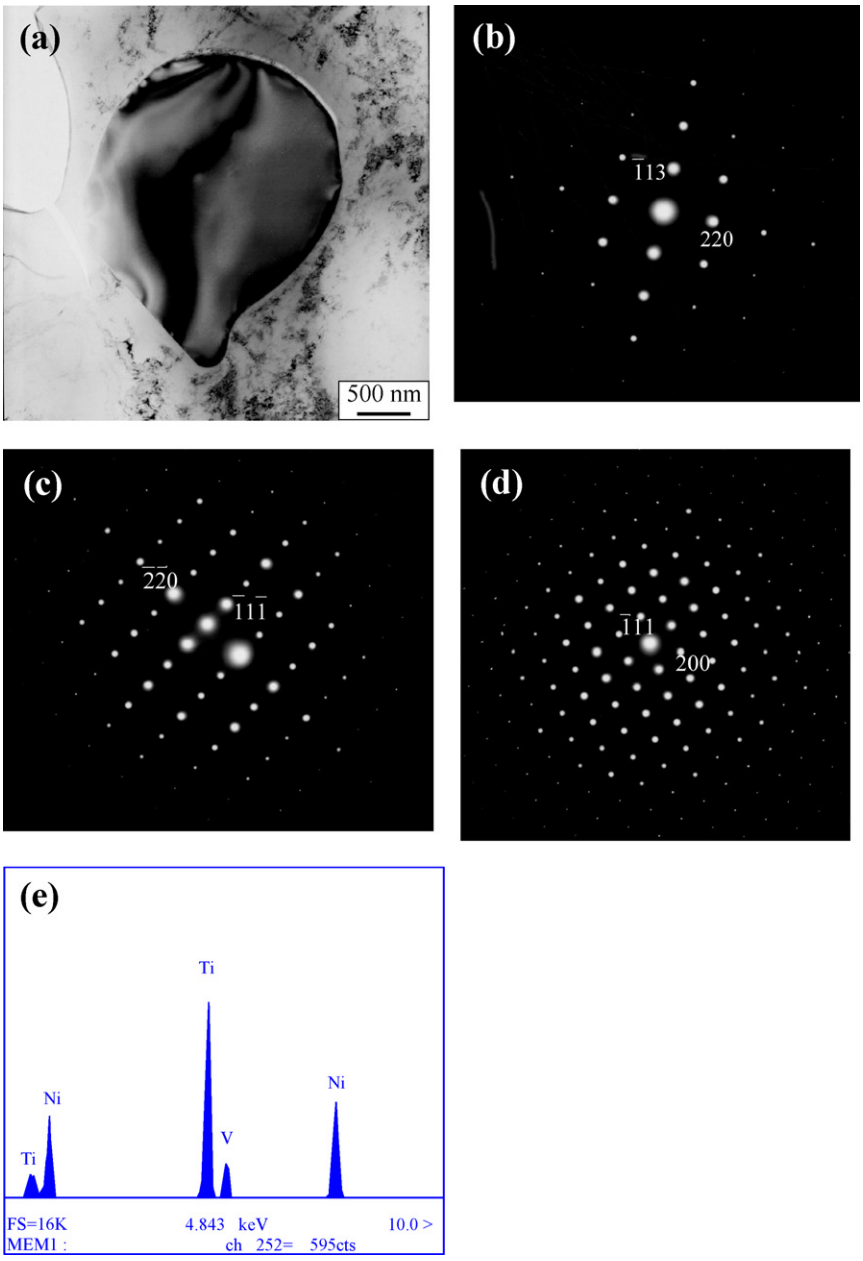

Fig. 3. TEM observation and SADP of A phase in the $Ti_{47.25}Ni_{48.75}V_4$ alloy. (a) Bright-field image, (b) $[3\,\bar{3}\,2]$ zone, (c) $[\bar{1}\,1\,2]$ zone, (d) $[0\,1\,\bar{1}]$ zone, and (e) TEM-EDS composition analysis.

the alloy's strength and shape memory effect. We are also interested to understand the precipitates of the 400 °C aged $Ti_{47.25}Ni_{48.75}V_4$ alloy in this study. Fig. 5(a–d) shows the bright-field image, SADP and TEM-EDS composition analysis of the 400 °C × 5 h aged $Ti_{47.25}Ni_{48.75}V_4$ alloy. In addition to the bigger particles of the A phase, there appear lots of fine spherical precipitates, about 100 nm, as indicated C in Fig. 5(a). According to the analysis of Fig. 5(b–d) and comparing to the results

Table 1
The structure, lattice parameter, compositions for A, B, C phases and specimen matrix

Phase	Compositions			Structure	Lattice parameter (Å)
	Ti	Ni	V		
A $(Ti,V)_2Ni$	61.14	34.79	4.07	FCC order	11.1
B $V_9(Ti,Ni)$	4.89	4.07	90.51	BCC	3.01
C $V_9(Ti,Ni)$	4.89	4.07	90.51	BCC	3.01
Specimen matrix	46.40	50.69	2.91	–	–

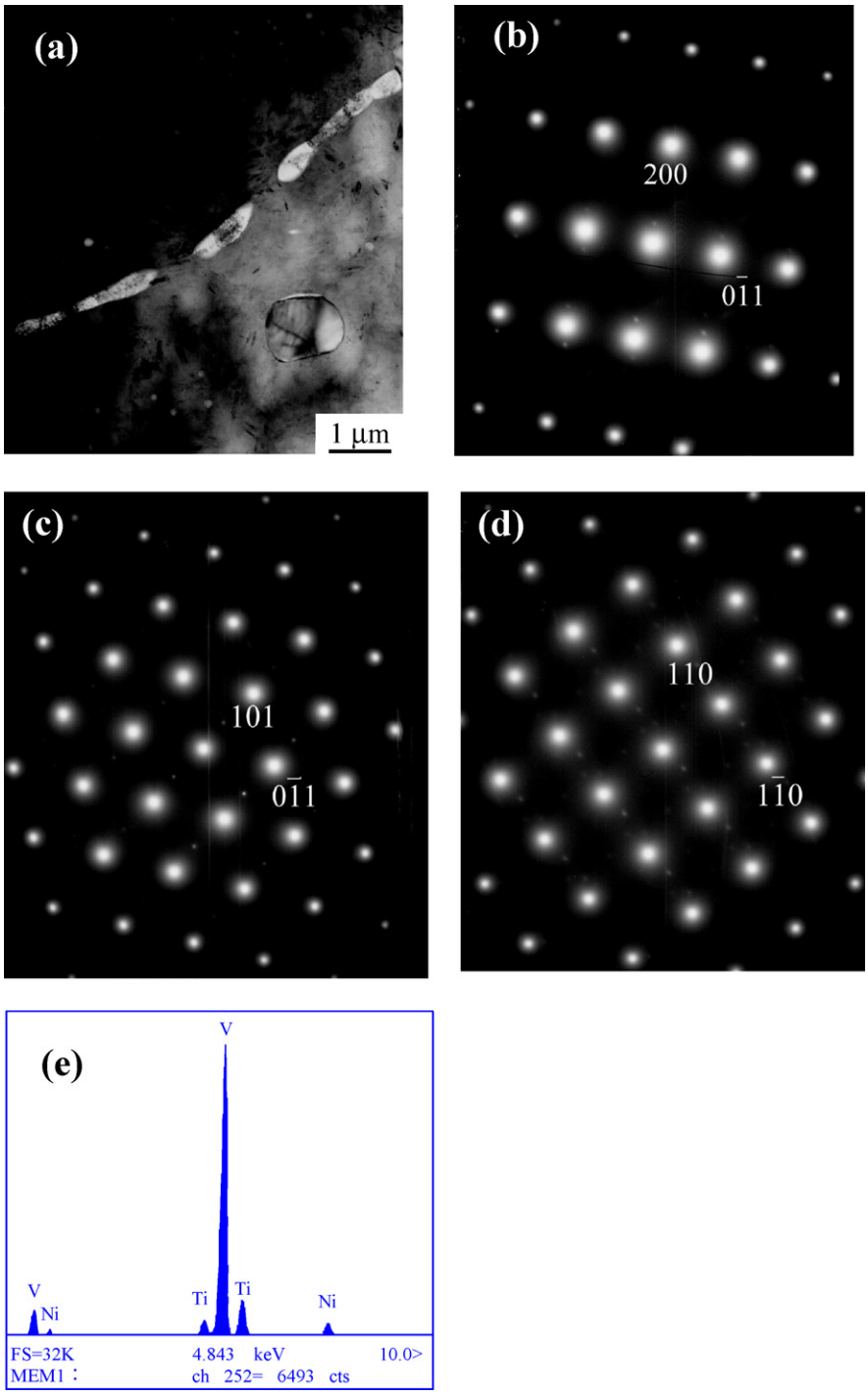

Fig. 4. TEM observation and SADP of B phase in the $Ti_{47.25}Ni_{48.75}V_4$ alloy. (a) Bright-field image, (b) [0 1 1] zone, (c) [1 $\bar{1}$ 1] zone, (d) [0 0 $\bar{1}$] zone, and (e) TEM-EDS composition analysis.

in Fig. 4(b–e), the C precipitate has the same structure, lattice parameter and compositions as those of B phase. This indicates that both B and C particles are V_9(Ti,Ni) phase, although they have different shape and size. The B phase is an equilibrium second phase, which forms at a higher temperature of solution treatment. These B particles will grow up rapidly along the grain boundaries. Whilst, the C phase is an aging precipitate, which forms at a lower aging temperature of 400 °C. Hence, the C particles grow up slowly and are mainly observed within the matrix. The structure, lattice parameter, compositions for all the A, B, C phases and specimen matrix are summarized in Table 1.

In order to understand if there appear the Ti_3Ni_4 precipitates in the 400 °C aged $Ti_{47.25}Ni_{48.75}V_4$ alloy. The TEM bright-field image is more magnified and shown in Fig. 6(a). The selected area diffraction pattern (SADP) is also presented in Fig. 6(b). As shown in Fig. 6(a), a lot of coherent precipitates are observed in the matrix. By comparing with the diffraction patterns of 400 °C aged $Ti_{49}Ni_{51}$ binary alloy [22], the 1/7-$\langle\bar{3}\,2\,1\rangle_{B2}$ spots in the

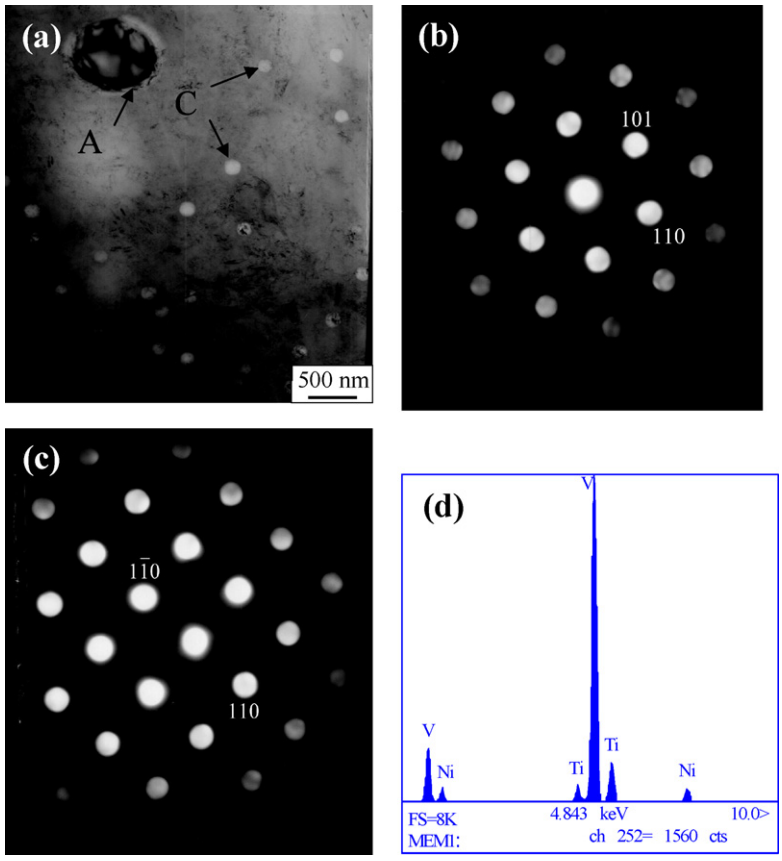

Fig. 5. TEM observation and SADP of C particles in the 400 °C × 5 h aged $Ti_{47.25}Ni_{48.75}V_4$ alloy. (a) Bright-field image, (b) [$\bar{1}$ 1 1] zone, (c) [0 0 1] zone, and (d) TEM-EDS composition analysis.

SADP of Fig. 6(b) demonstrate that these coherent precipitates are Ti_3Ni_4 precipitates. The formation of these Ti_3Ni_4 precipitates during 400 °C aging is predictable because the specimen matrix has Ni-rich compositions, although slight amount of V element exists, as presented in Table 1. The diffraction pattern of R-phase (1/3-$\langle 1\,0\,1\rangle_{B2}$ spots) can also be observed in Fig. 6(b). This feature indicates the existence of R-phase in the 400 °C aged $Ti_{47.25}Ni_{48.75}V_4$ alloy, and is consistent with the result of DSC measurement shown in Fig. 1.

3.3. Hardness and shape memory effect

Fig. 7 shows the specimen hardness and shape recovery versus aging time for the 400 °C aged $Ti_{47.25}Ni_{48.75}V_4$ alloy. In Fig. 7, the specimen hardness increases in the early stage of aging, reaches a maximum at 5 h, and then decreases with further aging. For the 400 °C aged $Ti_{47.25}Ni_{48.75}V_4$ alloy, both the V_9(Ti,Ni) and Ti_3Ni_4 precipitates will increase the specimen hardness, even up to 360 Hv, due to the precipitation hardening.

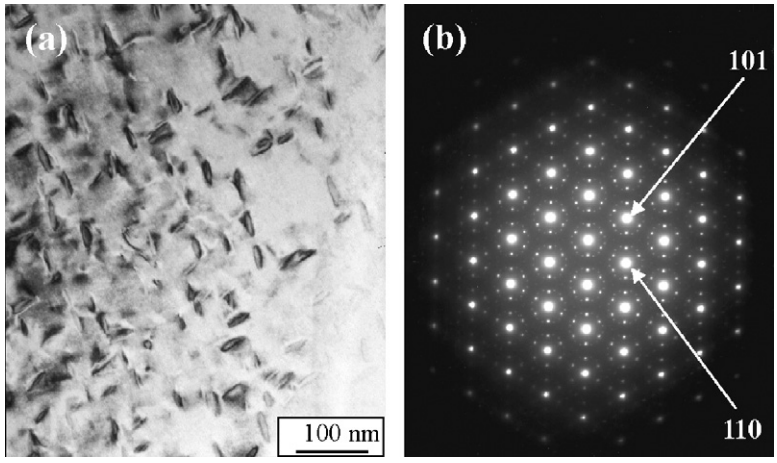

Fig. 6. TEM observation and SADP of the Ti_3Ni_4 precipitates in the 400 °C × 5 h aged $Ti_{47.25}Ni_{48.75}V_4$ alloy. (a) Bright-field image and (b) $[\bar{1}\ 1\ 1]_{B2}$ zone.

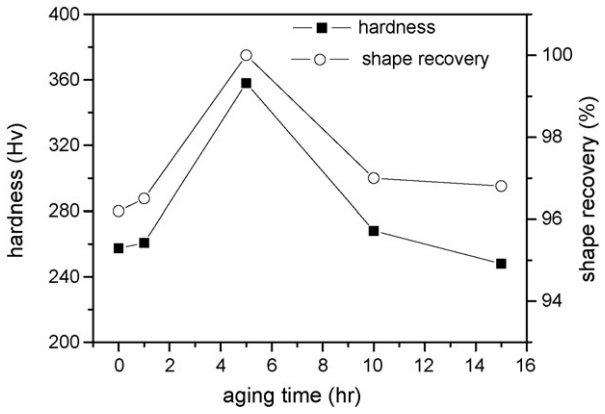

Fig. 7. The specimen hardness and shape recovery vs. aging time for the 400 °C aged $Ti_{47.25}Ni_{48.75}V_4$ alloy.

However, if the aging time is longer than 5 h, the phenomenon of over-aging appears and the specimen hardness decreases with further aging.

In Fig. 7, one can find that the variation of shape recovery with aging time has the same tendency as that of specimen hardness (which indicates the strength of specimen). Both the specimen hardness and shape recovery increase in the early stage of aging, reach the maximum values at 5 h, and then decrease in the over-aging period. As reported in our previous papers [9,15], the shape recovery of TiNi alloys increases with increasing cold-rolling or thermal cycling because these processes can strengthen the alloys. In other words, if the matrix is strengthened, the slip of dislocations is more difficult than the movement of twin boundaries during the application of external stress. Hence, the permanent plastic strain is reduced and the SME property is improved. In the present study, the V_9(Ti,Ni) and Ti_3Ni_4 precipitates in the 400 °C aged $Ti_{47.25}Ni_{48.75}V_4$ alloy will also strengthen the alloy and hinder the slip of dislocations, and hence the shape recovery ability can be significantly improved. The relationship between the specimen strength and shape recovery ability and the aging effect on the improvement of shape recovery ability are clearly presented in Fig. 7.

4. Conclusions

The aging effect on a $Ti_{47.25}Ni_{48.75}V_4$ shape memory alloy has been studied by using the DSC measurement, TEM observation, hardness and shape recovery tests. The important conclusions are as follows:

1. The $Ti_{47.25}Ni_{48.75}V_4$ alloy exhibits a B2 → R → B19′ two-stage martensitic transformation on cooling, but exhibits a B19′ → B2 one-stage transformation on heating after 400 °C aging. The transformation temperatures of the R-phase and martensitic transformations are found to slightly increase with increasing aging time, due to the variation of Ni/Ti ratio in the matrix after the aging treatment.
2. Two kinds of second phase, $(Ti,V)_2Ni$ and V_9(Ti,Ni), are observed in the solution-treated $Ti_{47.25}Ni_{48.75}V_4$ alloy. $(Ti,V)_2Ni$ exhibits an FCC order structure with a lattice parameter of 11.1 Å whereas V_9(Ti,Ni) exhibits a BCC structure with a lattice parameter of 3.01 Å.
3. There appear lots of fine spherical V_9(Ti,Ni) and coherent Ti_3Ni_4 precipitates after 400 °C aging for the $Ti_{47.25}Ni_{48.75}V_4$ alloy. These precipitates will strengthen the alloy's matrix and improve the shape recovery ability.

Acknowledgement

The authors are pleased to acknowledge the financial support of this research by National Science Council (NSC), Republic of China, under the NSC Grant 89-2216-E-035-018.

References

[1] S. Miyazaki, K. Otsuka, Y. Suzuki, Scripta Metall. 15 (1981) 287.
[2] S. Miyazaki, Y. Ohmi, K. Otsuka, Y. Suzuki, in: Proceedings of the ICOMAT-82, J. Phys. 43 (1982) C4–C255.
[3] S. Miyazaki, T. Imai, Y. Igo, K. Otsuka, Metall. Trans. A 17 (1986) 115.
[4] T. Tadaki, Y. Nakata, K. Shimizu, Trans. Jpn. Inst. Met. 28 (1987) 883.
[5] S. Miyazaki, Y. Igo, K. Otsuka, Acta Metall. 34 (1986) 2045.
[6] S.K. Wu, H.C. Lin, T.S. Chou, Acta Metall. 38 (1990) 95.
[7] S.K. Wu, H.C. Lin, Scripta Metall. Mater. 25 (1991) 1295.
[8] H.C. Lin, S.K. Wu, T.S. Chou, H.P. Kao, Acta Metall. Mater. 39 (1991) 2069.
[9] H.C. Lin, S.K. Wu, Acta Metall. Mater. 42 (1994) 1623.
[10] E.K. Eckelmeyer, Scripta Metall. 10 (1976) 667.
[11] P.M. Ossi, Mater. Sci. Eng. 77 (1986) L5.
[12] S.K. Wu, C.M. Wayman, Metallography 20 (1987) 359.
[13] Y.C. Lo, S.K. Wu, C.M. Wayman, Scripta Metall. Mater. 24 (1990) 1571.
[14] M. Piao, S. Miyazaki, K. Otsuka, Mater. Trans. J. Inst. Met. 33 (1992) 346.
[15] H.C. Lin, K.M. Lin, S.K. Chang, C.S. Lin, J. Alloys Compd. 284 (1999) 213.
[16] H.C. Lin, S.K. Wu, Scripta Metall. Mater. 26 (1992) 59.
[17] S. Miyazaki, K. Otsuka, Metall. Trans. A 17 (1986) 53.
[18] M. Nishida, C.M. Wayman, Metallography 21 (1988) 255, 275.
[19] M. Nishida, T. Honma, Scripta Metall. 18 (1984) 1299.
[20] T. Honma, Proc. SMA-86 (1986) 83.
[21] H.C. Lin, S.K. Wu, J.C. Lin, Mater. Chem. Phys. 37 (1992) 184.
[22] S.K. Wu, C.M. Wayman, Acta Metall. 37 (1989) 2805.